

Communication and Powering Scheme for Wireless and Battery-Less Measurement

Adam BOUŘA, Miroslav HUSÁK

Dept. of Microelectronics, Czech Technical University in Prague, Technická 2, 166 27 Prague 6, Czech Republic

bouaraar@fel.cvut.cz, husak@fel.cvut.cz

Abstract. *The paper presents solution for wireless and battery-less measurement in the enclosed areas. The principle is based on passive RFID; nevertheless this paper is focused on high power-demanding applications such as MEMS accelerometers, gas sensors, piezoresistive strain gauges, etc. Standard RFID communication scheme (sensing the input current change on the primary side) cannot be used in this case, because the communication channel is overloaded by the high power load. Paper presents possible solution which is based on the dual frequency scheme – one frequency for powering and other for the communication. This is ensuring capability for measurement up to several centimeters in the frequency bands 125 kHz and 375 kHz. It can be suitable for continual measurement in isolated systems such as the rotating objects, concrete walls, enclosed plastic barrels, high temperature chambers etc.*

Keywords

Wireless powering, wireless sensor, dual frequency, long-term monitoring.

1. Introduction

Measurement in the isolated systems is a crucial task in many areas of interest. Demand of wireless and battery-less powering can be caused by different reasons. Battery powering takes place when the powering wires cannot be guided to the sensor (e.g. rotating device, homogeneity of the surface ...). Unfortunately this is not suitable for every application. The main disadvantage of the battery powering is the limited lifetime and sometimes an improper environment for the battery (e.g. high temperature). In those cases the wireless powering must be applied.

Wireless powering can be performed for instance using the solar cells, temperature difference cells or harvesting the energy from vibrations. This paper focuses on the energy from the near magnetic field which is injected to the system. The coils are designed for surface mounting. This solution is proper for short distances only; typically several centimeters. The principle is similar to the

RFID systems. Modification of the standard RFID tag starts to be very popular [1], [2]. It allows adding some extra functionality to the standard RFID infrastructure. The basic principle is also used for powering and communication with isolated systems such as implantable probes for monitoring or stimulating devices [3], [4], [5].

The work presented in this paper is based on the standard RFID powering and communication scheme but it is more powerful and allows separated powering and communication on different frequencies. It allows a deeper modulation and thus bigger distances for signal detection. Presented principle is suitable for wireless measurement using the converters that have digital serial data output or with the signal output that can be used for driving the switch [6].

2. Basic Principle Description

When two or more inductors partly share the magnetic field, the coupling is presented. Fig. 1 shows an example of such coupling for arbitrary inductors. Voltage transferred to the second inductor can be calculated using the Faraday's law.

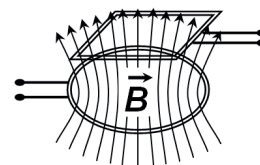


Fig. 1. Example of coupled inductors.

The secondary voltage thus depends on the secondary coils geometry and on the magnetic field distribution of the primary coil.

In terms of the circuit theory the inductive coupling can be described using the mutual inductance or using the coupling coefficient. This approach is suitable because the standard simulation tools can be used for a description of the powering. As well as the voltage transfer also the coupling coefficient is given by the coils geometry and the magnetic field distribution. The most important topology of the coils is the axial orientation according to Fig. 1. Coefficient's dependency versus the distance between the

coils is given by the distribution of the magnetic field intensity.

Circular coil of radius r , with negligible height, winding number N and current carrying I , induces the magnetic induction B (in environment of permeability μ_0). Axial component of the magnetic induction that can be measured on the axis which is perpendicular to the coil's area can be expressed by an equation (1) [7], where x stands for the axial distance.

$$B = \frac{\mu_0 \cdot N \cdot I \cdot r^2}{2 \cdot (r^2 + x^2)^{3/2}} \approx \frac{\mu_0 \cdot N \cdot I \cdot r^2}{2} \frac{1}{x^3} \Big|_{x \gg r} \quad (1)$$

The flux density drop is proportional to $1/x^3$ for distances much bigger than the coils diameter and thus also the coupling coefficient k is dependent this way. For smaller distances the coupling coefficient change is approximately exponential. Measurement result of the coupling coefficient between the circular coil and the rectangular surface coil is depicted in Fig. 2. This dependency is approximated using the exponential and the $1/x^3$ functions.

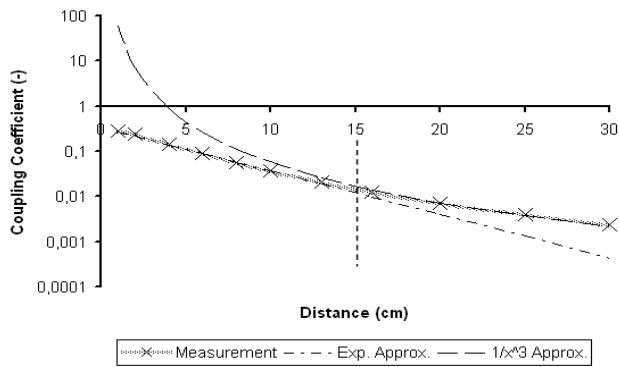


Fig. 2. Approximation of the coupling coefficient by the exponential and $1/x^3$ functions.

The character of this dependency is changing approximately at the distance equal to the diameter of the bigger coil (vertical dash line in the picture). Knowledge of the coefficient's character can be used for a prediction of its value for arbitrary coils.

2.1 Weakly Coupled Inductors

The mutual inductances from Fig. 1 can be described using the equations that relate the voltage phasors V_1 , V_2 , current phasors I_1 , I_2 , and loading impedance Z_L for the angular frequency ω . These basic equations can be used for derivation of the basic relationships in the circuit.

The most important parameter of the coupled inductors is the voltage transfer. It must be high enough to guarantee sufficient voltage level on the secondary side for rectification and for powering the sensing probe. The voltage transfer is affected by the parasitic properties of the coupled inductors – mainly by the inductor's serial

resistance. In presented application the parasitic resistance can be usually neglected. Equation (2) describes the voltage transfer for ideal inductors. Input impedance that can be seen on the primary inductor L_1 (3) [8] is important for the communication strategy. The input impedance depends on the loading impedance Z_L and on the coupling coefficient k .

$$\hat{V}_2 = \hat{V}_1 \cdot \frac{k \cdot \hat{Z}_L \cdot \sqrt{\frac{L_2}{L_1}}}{\hat{Z}_L + j\omega L_2 \cdot (1 - k^2)} \quad (2)$$

$$\hat{Z}_{in} = \frac{\hat{V}_1}{\hat{I}_1} = \frac{j\omega L_1 \cdot \hat{Z}_L + j\omega L_1 \cdot j\omega L_2 \cdot (1 - k^2)}{\hat{Z}_L + j\omega L_2} \quad (3)$$

The transformation of the Z_L to the input side is significant especially in resonance and variation of this impedance can be used for a signal transfer. This will be described in detail in next chapters.

2.2 Equivalent Circuit

It is helpful to derive an equivalent circuit (Fig. 3) of the coupled inductors for an understanding the effects in the circuit. Derivation of this circuit can be realized by observing the circuit's behavior under the loading impedance change [5].

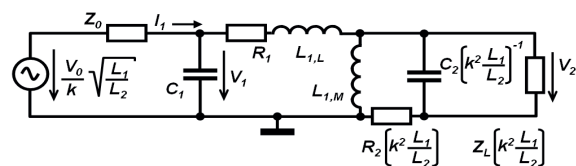


Fig. 3. Equivalent circuit which is respecting the parasitic properties of the inductors.

First, the secondary side can be presumed shorted ($Z_L \rightarrow 0$). According the (3) the input impedance is equal to (4) which represents an inductor $L_{1,L}$.

$$\lim_{Z_L \rightarrow 0} \hat{Z}_{in} = j\omega \cdot L_1 \cdot (1 - k^2) = j\omega \cdot L_{1,L} \quad (4)$$

This inductor is called the leakage inductor and it is characterized by the magnetic field excluding the secondary inductor. The magnetic field which contributes to the secondary side is represented by the magnetizing inductor $L_{1,M}$ - (5) [8].

$$L_{1,M} = L_1 \cdot k^2, \quad (5)$$

$$\hat{Z}_{L,e} = \hat{Z}_L \cdot \frac{L_1}{L_2} \cdot k^2 \quad (6)$$

Equation (6) describes the transformed loading impedance. Equivalent circuit thus consists of serial combination of the leakage inductor and the magnetizing inductor in parallel with the transformed loading impedance. Fig. 3 shows the equivalent circuit including

the parasitic properties of the coils such as the serial resistances R_1, R_2 and the parasitic capacitances C_1, C_2 . The capacitances are important for the powering and signal transfer strategy. In this case the capacitances are connected to the circuit intentionally and the parasitic capacities of the inductors are summed with them. In order to keep the circuit equivalent, also the input voltage must be transformed.

2.3 Resonance Behavior

It is evident from the Fig. 3, that the circuit must exhibit some resonant behavior. Omitting the parasitic resistances, the parallel resonance frequency f_{rp0} can be expressed using the (7). The inductor L_e is a parallel combination of the $L_{1,L}$ and $L_{1,M}$. Parallel capacitance C_p is the secondary side capacitance C_2 transformed using (6) (in this equation the C_p stands for the Z_L).

$$f_{rp0} = \frac{1}{2 \cdot \pi \sqrt{L_e C_p}} = \frac{1}{2 \cdot \pi \sqrt{L_2 \cdot C_2 \cdot (1 - k^2)}} \quad (7)$$

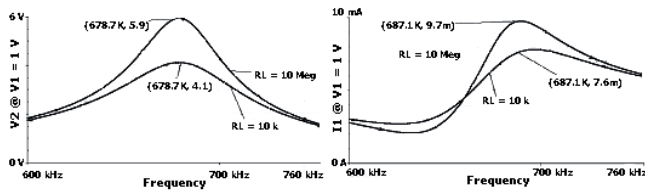


Fig. 4. Simulation according to Fig. 3, parallel resonance; $L_1 = 55 \mu\text{H}$, $L_2 = 82 \mu\text{H}$, $C_1 = 150 \text{ pF}$, $R_1 = 1.2 \Omega$, $R_2 = 21.4 \Omega$, $k = 0.34$; $C_2 = 758.4 \text{ pF}$.

The voltage transfer in resonance can exceed the nominal transfer (2) up to thousands of percent - see a graph in Fig. 4. This effect is crucial part of the powering strategy because the voltage level on the load must be high enough for rectification.

The serial resonance on the primary side can be also presented (impedance Z_0 from Fig. 3 must be a capacitor that resonates with $L_{1,L}$). This resonance increases the voltage transfer and it is more powerful for longer distances. Combination of both resonances is most suitable for long distance powering [9].

2.4 Principle of Communication

The voltage transfer in resonance is very sensitive on the loading impedance because it is changing the quality factor of the resonance tank circuit. The input current of the inductor L_1 is also changing according to the load (Fig. 4). This effect can be used for communication between the powered probe and the transmitting device. Simple powering and communication scheme is presented in Fig. 5.

The signal transfer from the sensing probe can be realized using the current measurement on the primary inductor. The input current is different for each position of

the switch because the modulating resistor R_m changes the quality factor. The loading impedance represented by the sensing probe is stable (or slowly changing) because of the filtering capacitor C_f . Thus current change on the input is caused mainly by the output signal from the probe.

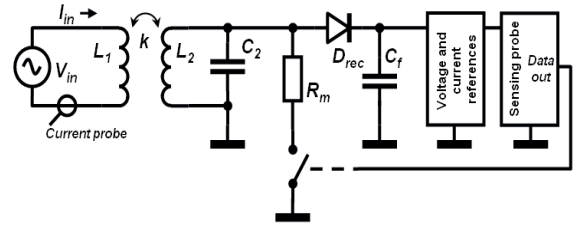


Fig. 5. Simplified powering and communication scheme.

Fig. 6 depicts an example of the signal transfer according to the presented scheme. Upper side of the figure describes the input current I_{in} and the bottom curve is the filtered voltage which can be used for the powering. Changes in amplitude of the signals are caused by the switched R_m of the value $10 \text{ k}\Omega$.

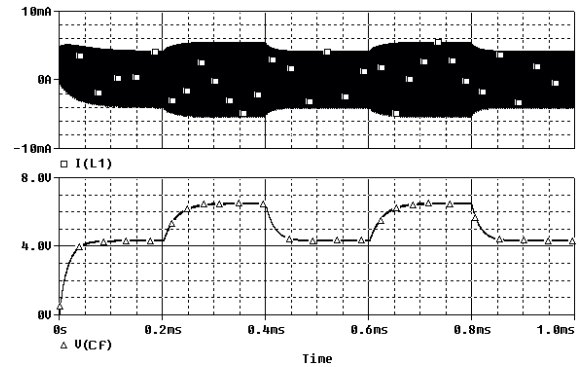


Fig. 6. Example of the powering and communication according the Fig. 5; upper graph is the current in the primary inductor L_1 ; bottom graph represents a secondary voltage on the filtering capacitor C_f .

The frequency of the input source must be tuned according to (7). For given inductors and given frequency it can be tuned using the capacitance C_2 . This capacitance is affected by the parasitic properties of the rectifying diode D_{rec} and capacity of the switch. It is advisable to use high frequency and low voltage-drop devices for this purpose such as Schottky diode for rectifying and bipolar junction transistor as the switch. Filtering capacitor C_f serves as the energy storage and its value does not affect the resonance frequency.

3. Principle Modification

When the power consumption of the sensing probe is too high, the presented simple powering and communication scheme cannot be applied. The consumption of the probe is drowning out the change of the modulating resistor and thus the communication is ineffective. The modulation can be accentuated by decreasing the resistor R_m , while the secondary voltage then also drops down and

the probe can be affected by this (see Fig. 6 – bottom curve). In order to solve the problem, it is important to separate the powering and the communication channels.

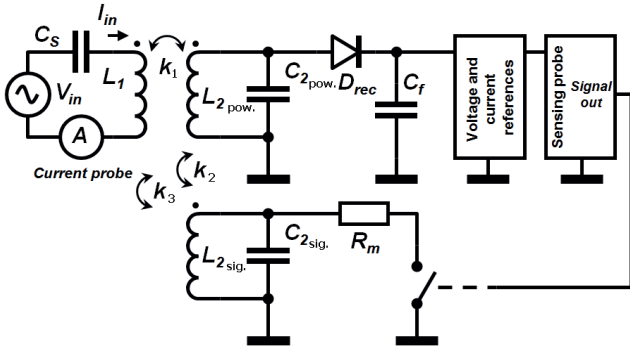


Fig. 7. Simplified scheme with separated channels for powering and communication.

The separation can be performed using splitting the operating time into two parts – time for collecting the energy and time for measurement and signal transmission. Other possibility is to divide the powering and communication channels by the frequency bands. Then, the measurement can be continual. Fig. 7 shows a modified RFID principle, where the powering and communication has its own receiving inductors and the frequencies can be different. This allows deeper modulation (up to short-circuit $R_m \rightarrow 0$) and thus bigger distance for detection.

The inductor L_{2pow} is powering the probe and the inductor L_{2sig} is used for the signal transfer. The coupling coefficient k_2 between the L_{2pow} , L_{2sig} is parasitic and should be minimal in order to keep the lines separated. Signal transfer from the sensing probe is sensed using the current probe on the inductor L_1 . If the resonance is present on the input side (L_1 , C_s), the current probe can be omitted and only the voltage on the inductor can be sensed. For each position of the switch, the input current is also different on given frequency, because the modulating resistor R_m changes the quality factor of the tank circuit L_{2sig} , C_{2sig} . The loading impedance represented by the sensing probe is stable and on different frequency. Thus the current change on the input side is caused mainly by the switch.

3.1 Coils

The crucial devices for maximizing the performance are the secondary coils. Fig. 8 presents two possible configurations. The overall geometry of the coils is demanded by the application. The surface mounting is presumed, thus the rectangular surface coils were tested. In the center, there is situated the sensing probe and the electronics. Two basic configurations were tested where the total surface of the coils was equal. Power and signal-transfer ability for both configurations are different.

If the axial configuration is used, the coupling coefficient between the secondary windings is 0.44. This is many times bigger than a typical coupling coefficient

between the transmitting and receiving coils. Because of big coupling coefficient between the receiving coils for the axial configuration, the modulating switch is affecting also the powering line and it is not effective. Thus this configuration is useless.

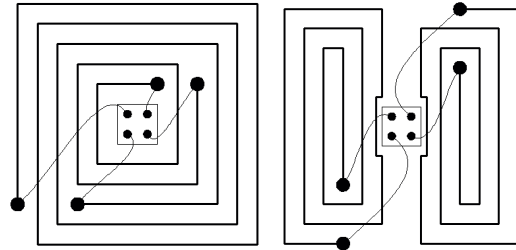


Fig. 8. Two possible configurations of the powering and signal coils, axial (left), side-by-side (right).

For side-by-side configuration, the performance of the powering is stable and nearly independent on the signal line. Coupling coefficient between the secondary windings is just 0.024. This ensures possibility of sensing the signal for long distances and simultaneously provides enough energy for powering. This configuration must be preferred in order to maximize the modulation depth (modulating switch can go up to short-circuit).

4. Simulation and Measurement Results

Tab. 1 presents coils that were used for practical measurements and simulations. The parasitic resistances of the coils are taken into account in simulation, but in practical applications it can be usually neglected as well as the parasitic capacitances.

Primary coil		Simple wound coil	
		Diameter:	13.5 cm
Secondary coils		Winding number:	18 turns
		Inductivity:	185 μ H
		Serial resistance:	1.2 Ω
		Parasitic capacitance:	150 pF
		Dual surface rectangular coils	
Diameter:		9 \times 4.5 cm (each)	
Winding number:		21 turns (each)	
Inductivity:		20.8 μ H (each)	
Serial resistance:		1.4 Ω (each)	
Coupling coefficient between the windings:		0.024	

Tab. 1. Coils used for experiments and simulations.

4.1 Simulation Scheme and Signal Strategy

Fig. 9 shows the simulation scheme of the powering and communication circuit. The parameters of the circuit were extracted from the real coils (Tab. 1) and the coupling coefficient between the primary and the secondary side was stated to be 0.2, which corresponds to a distance of 4 cm

(see the graph in Fig. 2). The capacitors were calculated in order to create the resonant tank circuits on desired frequencies. Resistor R_{load} represents an equivalent resistance of the rectifier and powering for the sensing probe and its value is constant. Resistor R_m represents the modulating resistor. Resistor R_l is the parasitic property of the inductor L_l . Resistor R_i represents an internal resistivity of the voltage source.

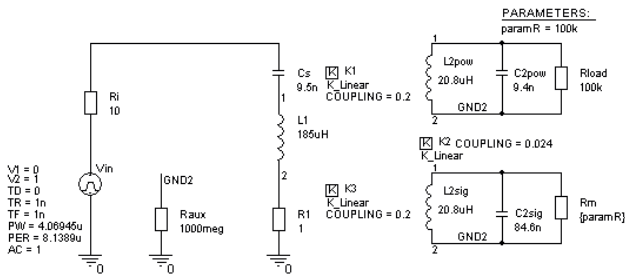


Fig. 9. Simulation scheme of the modified circuit according to Fig. 7.

If the primary serial resonance is presented (L_l, C_s), the selection of the frequency bands is easy. The communication frequency is given by this resonance and the odd multiple of the basic frequency can be selected for powering (for instance the 3rd harmonic).

Construction of the primary voltage source is very simple – only a switch that is producing the rectangular waveform. Resistor R_i represents its resistivity when it is ON-state.

Equation (8) expresses the harmonics forming the square signal. Serial resonance on the input (L_l, C_s) and the parallel resonance on the L_{2sig}, C_{2sig} should be tuned on the first harmonic. This frequency channel is for communication. The tank circuit L_{2pow}, C_{2pow} is tuned on the third harmonic and serves for the powering.

$$u_0(t) = U_m \cdot \frac{4}{\pi} \cdot \sum_{n=1,3,5,\dots}^{\infty} \left[\frac{1}{n} \cdot \sin(n \cdot 2 \cdot \pi \cdot f \cdot t) \right] \quad (8)$$

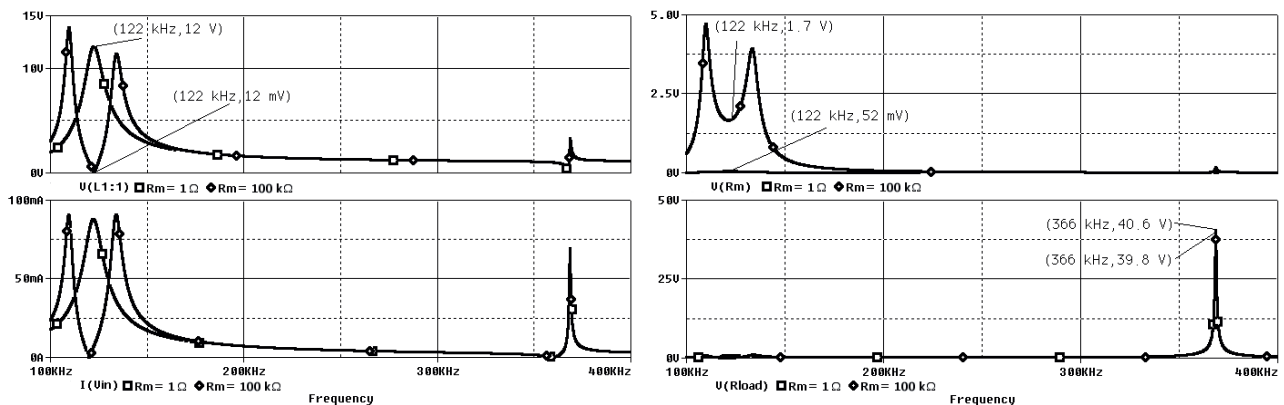


Fig. 10. AC analyze of the input (left side) and output (right side) voltages and current.

It is also possible to use the 1st harmonic for powering and the 3rd harmonic for communication. This configuration is advisable especially for high demanding powering because the first harmonic has the biggest amplitude. The limitation is then caused mainly by the signal detection problem. The 3rd harmonic has smaller amplitude, thus the sensitivity is smaller. Moreover, an extra band-pass filter must be implemented for the evaluation circuit. This is not necessary in case when the 1st harmonic is used for the communication. The current change in the inductor L_l is proportional to the change of its voltage (see Fig. 11 in next chapter). The voltage is increased by the serial resonance L_l, C_s and it is many times bigger than the 3rd harmonic frequency. This is why the preferable configuration is the 1st harmonic for communication and the 3rd harmonic for powering. This configuration was used for simulations and real measurements.

The parametric simulation was performed. The parameter was the resistor R_m . Its values were 1 Ω and 100 k Ω which simulated the modulating switch.

4.2 Simulation Results

Circuit from Fig. 9 was simulated in the SPICE program. Fig. 10 presents the AC results for input and output voltages and currents. On the left side the voltage on the inductor L_l is presented (top) and also the input current (bottom). The voltage on the first harmonic frequency 122 kHz is changing with the load R_m which is desired. This voltage is used for signal detection. On the right side of Fig. 10, the voltages of the secondary tank circuits are presented. Voltage on the modulating resistor R_m (top) is changing, even though it is not important. The voltage on the powered load R_{load} (bottom) is stable and it is only slightly changing with the resistor R_m . It is ensured by low value of the coupling coefficient k_2 .

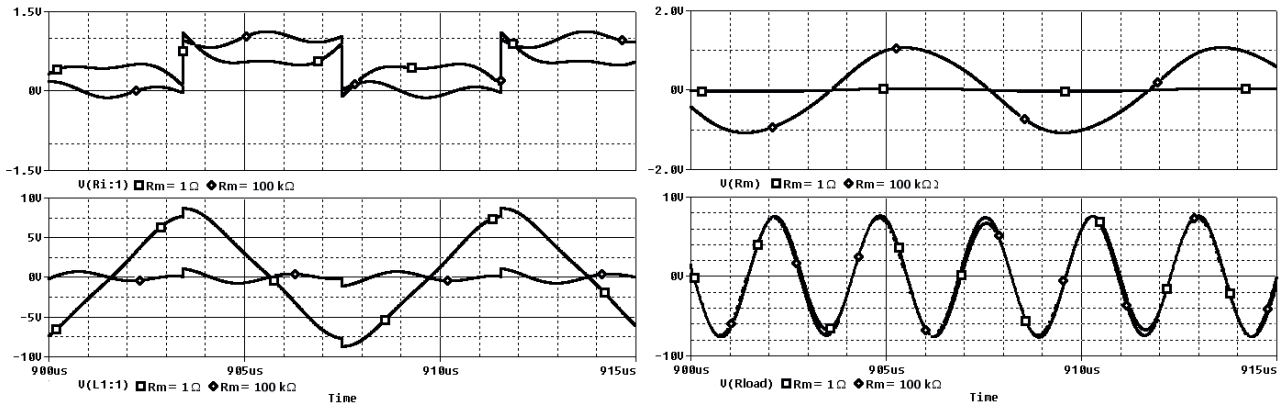


Fig. 11. Transient analyze of the input (left side) and output (right side) voltages.

Transient analysis of the voltages is presented in Fig. 11. The circuit was simulated with square voltage on the input side. Basic frequency was 122 kHz. Again, the voltages are studied for two values of the resistor R_m (1Ω , $100 \text{ k}\Omega$). The top-left waveform is the input voltage. The shape is deformed because of the internal resistance R_i (rectangular voltage source) and harmonic loading current.

The voltage on the inductor L_1 (bottom-left) is changing with the resistor R_m as it was in AC analysis. The voltage peak detector can be used for signal reception instead of the current probe from Fig. 7. Voltages on the output sides are in agreement with the AC analysis. Only the absolute values of the voltage levels are different because of the input voltage character. For AC analyses the input voltage has amplitude 1 V for every frequency. Amplitude of the input square signal in transient simulation is 1 V which is equivalent to 0.5 V of the AC signal. The third harmonic of the input voltage should have amplitude of 0.21 V (8), but the internal resistance R_i of the voltage source (switch) is lowering it slightly. As the result, the voltage on the R_{load} is about 5 times lower for transient simulation compared to the AC simulation. The voltage for powering (Fig. 11 bottom right curve) is tuned by the parallel resonance and it is stable with the change of the R_m resistor. Voltage on the modulating resistor (Fig. 11 top right curve) is irrelevant.

Presented scheme is optimized for powering the equivalent load of $31 \text{ k}\Omega$. Maximal power that can be delivered to the load is 22.5 mW (for $V_{in} = 1 \text{ V}$).

4.3 Comparison with Measurement

In real measurement, the resonant tank circuits were slightly unbalanced – namely because of the parasitic effect of the oscilloscope probes and other wires. This is why the voltages and phase shifts are not precisely according to the simulation, while the overall results are corresponding. Fig. 12 left is presenting signals that were measured on the testing circuit and that are comparable with the Fig. 11. Voltage levels are different, because the real circuit was loaded by the sensing probe and the modulating resistor was different as it was in the simulation.

Fig. 12 is presenting four channels. Channel 1 of the oscilloscope shows the input voltage for weakly loaded output and it corresponds to the top-left curve from Fig. 11. Channel 2 shows the voltage on the inductor L_1 and corresponds to Fig. 11 bottom-left curve. This voltage is used for sensing the signal from the probe. Channel 3 represents to the voltage on the modulating resistor R_m (corresponds to Fig 11, top-right). Finally, channel 4 represents the voltage which is powering the sensing probe (corresponds to Fig 11, bottom-right).

The communication strategy was proved using the circuit consisting of discrete transistors (Fig. 12 right). The circuit was used for powering and communication with the MEMS sensors and devices.

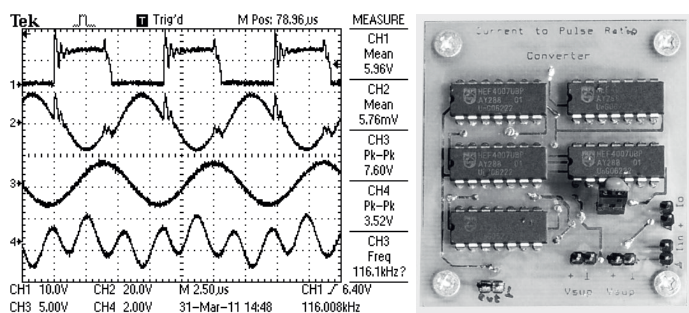


Fig. 12. Real measurement results (left), realization of the sensing probe using the discrete devices (right).

5. Conclusion

The paper presented wireless powering solution for measurement in the isolated areas which can be used for long-term monitoring of contamination or physical damage in barrels, concrete walls, measurement on the rotating objects etc. It is provided by the near magnetic field and the signal transfer principle is similar to the RFID systems. The possibility of maximizing the power transfer is presented. It allows performing the high power measurement (high power comparing the RFID systems). The paper is focused on dual frequency solution – one frequency for powering, other for the signal transfer. It can deliver up to several milliwatts on distance of several centimeters (frequency bands 125 kHz and 375 kHz). Functionality of the system was tested on the circuit consisting of discrete devices and the setup is able to read output from the accelerometer ADXL203 and the strain gauges. The measurement was effective up to distances of 10 cm. Nowadays, an integrated circuit is designed. Expected performance is 15 cm distance ability and the accuracy better than 5 %.

Acknowledgements

Research described in the paper has been supported by the Czech Science Foundation project No. 102/09/1601 “Micro- and nano-sensor structures and systems with embedded intelligence” and partially by the Ministry of Interior research program No. VG20102015015 – “Miniature intelligent system for analyzing concentrations of gases and pollutants, particularly toxic” (2010-2015, MV0/VG).

References

- [1] IDS Microchip AG. *IDS-SL13A, Smart Label Chip with Sensor For Unique Identification, Monitoring and Data Logging*, datasheet. [Online] 2008 Available at: http://www.ids.si/doc/sd/SL13A_SD.pdf
- [2] ŠTRAUS, D., KOVAČIČ, K. Self-heating compensation in temperature sensor RFID transponders. *Informacije MIDE M*, 2010, vol. 40, no. 2.
- [3] CHO, S., SON, S., CHUNG, H. LEE, J. A wireless powered fully integrated SU-8-based implantable LC transponder. *Microsystem Technologies*, 2010, vol. 16, no. 8-9, p. 1657 – 1663.
- [4] CATRYSSE, M., HERMANS, B., PUER, R. An inductive power system with integrated bi-directional data-transmission. *Sensors and Actuators A: Physical*, 2004, vol. 115, no. 2-3, p. 221 – 229.
- [5] WU, J., QUINN, V., BERNSTEIN, G. A simple, wireless powering scheme for MEMS devices. *MEMS Components and Applications for Industry, Automobiles Aerospace, and Communications, Proceedings of SPIE*, 2001, vol. 4559, p. 43 – 52.
- [6] HÁZE, J., VRBA, R., FUJCIK, L., FOREJTEK, J., ZAVORAL, P., PAVLÍK, M. Bandpass Sigma-Delta modulator for capacitive pressure sensor, In *IEEE Instrumentation and Measurement Technology Conference Proceedings*. Warsaw (Poland), 2007. p. 18 – 23.
- [7] PROCHAZKA, T. Antennas for RFID systems. *Elektrorevue*, 2002, vol. 22 [Online] Cited 2009. Available at: <http://www.elektrorevue.cz/clanky/02022/index.html>.
- [8] BOURA, A., KULHA, P., HUSAK, M. Simple wireless A/D converter for isolated systems. In *IEEE International Symposium on Industrial Electronics, ISIE 2009*. Seoul (Korea), 2009, p. 323 – 328.
- [9] BOURA, A., KULHA, P., HUSAK, M. Applicability of the inductive powering for enclosed systems and data transfer. In *Proceedings of 45th international conference on microelectronics, devices and materials MIDE M 2009*. Postojna (Slovenia), 2009, p.141 – 146.

About Authors ...

Adam BOUŘA was born in Ostrava in 1980. He graduated in Microelectronics from the FEE-CTU in Prague in 2004. Since 2004 he is a Ph.D. student at the Department of Microelectronic and member of the Microsystems group. His work is concentrated on wireless sensor systems.

Miroslav HUSÁK was born in Kladno in 1953. He graduated in Radioengineering from FEE-CTU in Prague in 1978. Ph.D. in 1985, Assoc. Professor in 1997, Full Professor in 2000. His research is concerned on microsystems and integrated sensor systems.